Journal of Power Sources 196 (2011) 3048–3053

Contents lists available at ScienceDirect

Journal of Power Sources

journal homepage: www.elsevier.com/locate/jpowsour

Sulfated SnO_2 modified multi-walled carbon nanotubes – A mixed proton–electron conducting support for Pt catalysts in direct ethanol fuel cells

Xinwei Zhang[a], Hong Zhu[b,*], Zhijun Guo[a], Yongsheng Wei[a], Fanghui Wang[b]

[a] Department of Chemistry, School of Science, Beijing Jiaotong University, Beijing 100044, PR China
[b] Institute of Modern Catalyst, State Key Laboratory of Chemical Resource Engineering, School of Science, Beijing University of Chemical Technology, Beijing 100029, PR China

ARTICLE INFO

Article history:
Received 16 November 2010
Accepted 20 November 2010
Available online 26 November 2010

Keywords:
Ethanol oxidation
Sulfated tin oxide
Electrocatalyst
Proton conductivity

ABSTRACT

We report on the synthesis of sulfated SnO_2 modified multi-walled carbon nanotubes (MWCNTs) composites as new supports of Pt catalyst (Pt–S-SnO_2/MWCNTs) with the aims to enhance electron and proton conductivity and also catalytic activity for ethanol oxidation. The Pt–S-SnO_2/MWCNTs catalyst is synthesized by a combination of improved sol–gel and pulse-microwave assisted polyol methods. The surface presence, morphology and structure of the Pt–S-SnO_2/MWCNTs catalyst are characterized by Fourier transform infrared spectroscopy (FT-IR), high-resolution transmission electron microscopy (HRTEM) and X-ray diffraction (XRD), respectively. The electrocatalytic properties of the Pt–S-SnO_2/MWCNTs catalyst for ethanol oxidation reactions are investigated by cyclic voltammetry, chronoamperometry and electrochemical impedance spectroscopy. The results show that Pt–S-SnO_2/MWCNTs catalyst exhibits higher catalytic activity for ethanol oxidation than Pt supported on non-sulfated SnO_2/MWCNTs composites.

1. Introduction

Direct ethanol fuel cell (DEFC) is considered a highly promising power source because ethanol offers higher theoretical energy density (8 kW h kg^{-1}) and lower toxicity than methanol (6.1 kW h kg^{-1}) [1–4]. Also, ethanol can be easily produced in large quantities from agricultural products or biomass [5,6]. However, the complete oxidation of ethanol is more difficult than that of methanol because the former requires the cleavage of C–C bonds. Ethanol oxidation undergoes both parallel and consecutive oxidation reactions, which produce a number of intermediates such as –CO–CH_3, –OCH_2–CH_3, =COH–CH_3 and linearly bonded CO [7]. It is well known that unmodified platinum catalysts are prone to poisoning in a DEFC because of the strongly adsorbed species coming from the intermediates of ethanol oxidation reaction. Therefore, the discovery of an effective catalyst with high ethanol oxidation reaction activity is a key research objective in the development of DEFCs. Up to now, many studies have shown that Pt-based catalysts decorated with metal oxides such as RuO_2–IrO_2 [8], MgO [9], CeO_2 [10], WO_3 [11], $Ce_xZr_{1-x}O_2$ [12], TiO_2 [13], ZrO_2 [14], and SnO_2 [15] have significant promotion effect on the catalytic activity and stability for the ethanol oxidation reactions. Of these metal oxides, tin oxide plays an active role in ethanol oxidation according to a bifunctional mechanism (Pt absorbs ethanol and oxidizes H, while SnO_2 supplies oxygen-containing species to oxidize the blocking intermediate CO) [16–19]. In a previous study, we investigated a Pt/(CNT@SnO_2) catalyst prepared by the sol–gel and ethylene glycol reduction methods and found that a thin SnO_2 layer acted as an efficient co-catalyst with Pt for ethanol oxidation [20]. However, tin oxide is semiconducting oxide and has low electric conductivity. The Pt nanoparticles deposited on the surface of a thicker SnO_2 layer or larger SnO_2 particles, which may be useless due to poor conductivity. On the other hand, the large SnO_2 particles with small surface area usually result in the poor dispersion of Pt nanoparticles. Therefore, an ideal support with high electron and proton conductivity is required to not only improve the catalytic activity, but also increase the utilization of Pt catalysts.

Mixed-conducting materials, combining a proton conductor and an electron conductor, may be an ideal catalyst support for ethanol oxidation because they transport protons and electrons at the same time, which should render a large portion of catalytic sites effective. Solid superacids, because of their strong acidity and water affinity, have attracted great attention as good fillers for Nafion membrane [21–24]. Sulfated SnO_2, also known as SO_4^{2-}–SnO_2 solid superacid, has relatively small particle size, high proton conductivity and good hydrophilic capacity due to the SO_4^{2-} group on the SnO_2 surface [25,26]. It is considered an ideal second catalyst (co-catalyst) for ethanol electro-catalyst. Carbon nanotubes are of interest as catalyst supports for fuel cells due to their unique electrical and structural properties [13,14,19,20]. However, up to now, sulfated SnO_2 has never been explored as a modifier for composite catalyst support for ethanol oxidation. With the aim of providing

* Corresponding author. Tel.: +86 10 64444919; fax: +86 10 82161887.
E-mail address: zhuho128@126.com (H. Zhu).

0378-7753/$ – see front matter Crown Copyright © 2010 Published by Elsevier B.V. All rights reserved.
doi:10.1016/j.jpowsour.2010.11.129

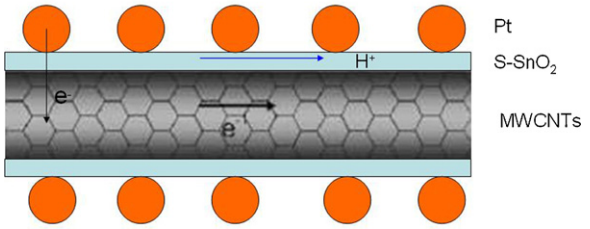

Fig. 1. Schematic diagram of the structure of the Pt–S-SnO_2/MWCNTs catalyst.

additional acidic sites to enhance proton transport, we exploited sulfated SnO_2 as a modifier for the S-SnO_2/MWCNTs composites.

In the present work, we successfully synthesized sulfated SnO_2 modified multi-walled carbon nanotubes composites as a new support of Pt catalysts (Pt–S-SnO_2/MWCNTs) for ethanol oxidation. The Pt–S-SnO_2/MWCNTs catalyst was synthesized by a combination of the improved sol–gel and pulse-microwave assisted polyol methods. The special catalyst structure (see Fig. 1) will increase the catalytic activity and utilization of Pt catalysts due to the high proton conductivity of sulfated SnO_2. The materials were characterized by Fourier transform infrared spectroscopy (FT-IR), X-ray diffraction (XRD), high-resolution transmission electron microscopy (HRTEM). Cyclic voltammetry (CV), chronoamperometry and impedance spectroscopy were used to evaluate their catalytic activities and durability for ethanol oxidation.

2. Experimental

2.1. Synthesis of S-SnO_2/MWCNTs supported Pt catalyst (Pt–S-SnO_2/MWCNTs)

S-SnO_2/MWCNTs composites were prepared by an improved sol–gel method, which was derived from the procedure presented by our group [20] and Matsuhashi et al. [25,26]. The primary steps of this synthesis process are as follows: (1) the as-received MWCNTs were first treated by refluxing in nitric acid (40%) at 110 °C for 2 h to improve their dispersibility in aqueous solution by forming oxygen-containing functional groups on their side walls. Acid-treated MWCNTs (10 mg) were added to 40 mL distilled H_2O followed by ultrasonication for 5 min. HCl (38%, 0.7 mL) was added during the ultrasonication. Then 1 g of hydrous $SnCl_2$ $2H_2O$ was added, and the solution was stirred for 2 h at room temperature. Finally, the sediments were filtrated. (2) The precipitated product was mixed with 4 wt% CH_3COONH_4 for 4 h. The suspension was filtered by suction, and the residue was collected and dried at 100 °C for more than 24 h. (3) The obtained solid was ground and then treated with 3 M H_2SO_4 solution at room temperature for 30 min, followed by filtration at room temperature and drying of the residue at 100 °C overnight. The dried residue was calcined at 500 °C under flowing N_2 for 3 h to form the S-SnO_2/MWCNTs composites. For comparison, SnO_2/MWCNTs composites were also prepared according to the above procedure without the treatments with CH_3COONH_4 solution and H_2SO_4 solution.

Pt–S-SnO_2/MWCNTs catalysts were prepared by the pulse-microwave assisted polyol method [27]. Appropriate H_2PtCl_6 $6H_2O$ ethylene glycol solution was well mixed with NaOH ethylene glycol solution. Ethylene glycol was used as a stabilizer and reducing agent. S-SnO_2/MWCNTs composites were then added to the mixed solution and sonicated for 45 min. A well-dispersed slurry was formed and microwave-heated in the form of pulse every 10 s for several times. The reaction mixture was cooled to room temperature; hydrochloric acid was adopted as the sedimentation promoter. A black solid sample was obtained after filtration, washed and dried at 80 °C for 10 h in a vacuum oven. For comparison, Pt–SnO_2/MWCNTs catalysts were also prepared by the same process. The nominal loading of Pt in the catalysts was 20 wt%.

2.2. Physical characterization

The morphology of the catalysts was characterized by high-resolution transmission electron microscopy (HRTEM, JEOL Model JEM-3010) at 300 kV. Power X-ray diffraction (XRD) patterns for the samples were obtained on a Rigaku D/MAX-RB diffractometer using Cu Ka radiation (λ = 0.15406 Å) and operating at 40 kV and 40 mA. The 2θ angular regions between 15° and 85° were investigated at a scan rate of 6° min^{-1} at 0.02° increments. The Fourier transform infrared (FT-IR) spectra were recorded in the range of 4000–400 cm^{-1} on a Nicolet 5700 spectrometer (Thermo, USA). Each spectrum was an average of accumulation of 32 scans at a resolution of 4 cm^{-1}.

2.3. Electrochemical measurements

All electrochemical measurements were performed at room temperature (T = 25 °C) by using an IM6e electrochemical workstation (Zahner-Electrik, Germany) in a standard three-electrode cell with a saturated calomel electrode (SCE) and a platinum foil (1.5 cm^2) as the reference electrode and the counter electrode, respectively. A glassy carbon electrode (GC Φ = 4 mm) sealed by poly (tetrafluoroethylene) was used as the working electrode. All potentials reported in this paper are versus SCE. The thin film working electrode was prepared by dispersing 10.0 mg catalyst in 4 mL ethanol and 0.1 mL Nafion solution (2.5 wt%) under ultrasonication for 45 min. The well-dispersed catalyst ink (10 μL) was transferred onto the pre-polished glassy carbon (GC) disk electrode by using a micropipette and dried under an infrared lamp. Before measurements, all electrodes were completely activated to a steady state by cyclic voltammetry (50 cycles) in a 0.1 M $HClO_4$ solution at a scan rate of 50 mV s^{-1} and a potential ranging from −0.241 to 0.959 V. The catalytic activities of the as-prepared catalysts were studied by cyclic voltammetries in a nitrogen saturated 0.1 M $HClO_4$ + 0.5 M CH_3CH_2OH solution at a scan rate of 50 mV s^{-1}, with potentials ranging from −0.241 to 0.959 V. The chronoamperometry tests were carried out at 0.4 V for 1000 s. The electrochemical impedance spectroscopy measurements of the samples were performed at a potential of 0.5 V in the frequency range of 100 kHz–0.1 Hz. Pt–SnO_2/MWCNTs was also tested by using identical procedures of electrode preparation and electrochemical activity.

3. Results and discussion

3.1. IR spectra analysis of S-SnO_2/MWCNTs composites

The FT-IR spectra of the S-SnO_2/MWCNTs and SnO_2/MWCNTs composites are presented in Fig. 2.The spectra were used to investigate the structure of sulfur on SnO_2 nanoparticles. The IR peaks observed in the region of 600–620 cm^{-1} are associated with Sn–O; similar observations were reported by Guo et al. [28] and Lam et al. [29]. Several absorption peaks in the 800–1300 cm^{-1} region were observed in the spectrum of the S-SnO_2/MWCNTs, but not in the spectrum of the SnO_2/MWCNTs. These characteristic absorption peaks were assigned to S=O or S–O bonds, which imply the presence of a high concentration of SOx bonded tightly with Sn that could result in high proton conductivity. All of these bands are related to the sulfate bound to the metal oxide in the chelate form as was observed in the case of other superacids [30]. A strong and broad band detected in the region of 3200–3600 cm^{-1} in curve (b) of Fig. 2 is assigned to the presence of physisorbed and coordinated water (–OH bond) on the S-SnO_2/MWCNTs composites [29]. It is well known that the oxidation of CO requires an adsorbed

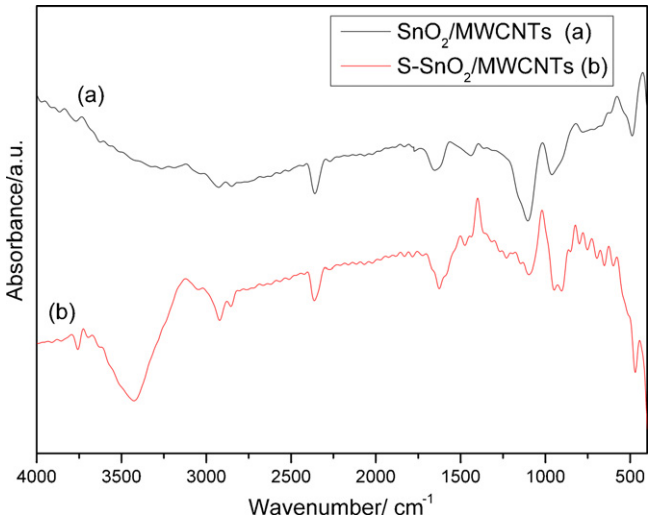

Fig. 2. FT-IR spectra of (a) SnO_2/MWCNTs and (b) S-SnO_2/MWCNTs composites.

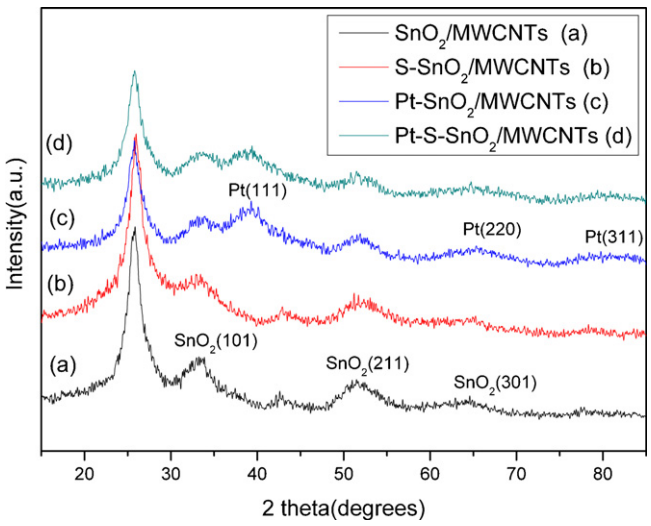

Fig. 4. XRD patterns of (a) SnO_2/MWCNTs, (b) S-SnO_2/MWCNTs, (c) Pt–SnO_2/MWCNTs and (d) Pt–S-SnO_2/MWCNTs composites.

OH species adjacent to the adsorbed CO. Sulfated SnO_2 can adsorb and dissociate more water than non-sulfated SnO_2, which produces more hydroxyl groups. Thus the COads are much easier to be oxidized, releasing the active sites of Pt for further electrochemical reaction [20].

3.2. TEM analysis of Pt–S-SnO_2/MWCNTs composites

Fig. 3 shows the typical TEM and HRTEM images of the Pt–S-SnO_2/MWCNT composites. It can be seen that fine Pt nanoparticles are homogeneously dispersed on the surface of S-SnO_2/MWCNTs without aggregation. The hollow structure of the MWCNTs was not clearly visible indicating that the sulfated SnO_2 coating was present on the MWCNTs as shown in the low-resolution TEM image. The HRTEM micrograph reveals further that Pt and S-SnO_2 nanoparticles attached on the sidewalls of the MWCNTs and the coating is rather uniform and thin. These phenomena were also observed in SnO_2/MWCNTs composites, as we reported before [20], and indicate that washing with the acetate solution and sulfating with H_2SO_4 solution do not destroy the structure of SnO_2/MWCNTs composites. The mixed proton–electron conducting materials, S-SnO_2/MWCNTs composites, have been successfully synthesized by a sol–gel reaction followed by sulfation and calcination procedures to form a new support for Pt catalysts (Pt–S-SnO_2/MWCNTs) in DEFCs. The diameter of the Pt particles is about only 2–5 nm with a mean value of 3.0 nm. Pt and S-SnO_2 nanoparticles can be easily identified from the crystal lattice pattern. The presence of Pt and S-SnO_2 nanoparticles can be further confirmed in the XRD results. Because sulfated SnO_2 has acid sites over the surface, these Pt catalysts support on S-SnO_2 layer can donate and accept protons in ethanol oxidation reaction, increasing the utilization of Pt catalyst.

3.3. XRD analysis of the Pt–S-SnO_2/MWCNTs composites

Fig. 4 displays the XRD patterns of Pt–S-SnO_2/MWCNTs and S-SnO_2/MWCNTs compared with those of Pt–SnO_2/MWCNTs and SnO_2/MWCNTs. The diffraction peaks of Pt, S-SnO_2 and SnO_2 can be observed in both the patterns of Pt–S-SnO_2/MWCNTs and Pt–SnO_2/MWCNTs catalysts, indicating their coexistence in the samples. The diffraction peaks at ca. 40°, 68°, and 81° can be ascribed to the (1 1 1), (2 2 0), and (3 1 1) planes of the face-centered cubic (fcc) structure of platinum. And there is no shift in any of the diffraction peaks of platinum in the Pt–S-SnO_2/MWCNTs and Pt–SnO_2/MWCNTs catalysts, indicating that the addition of S-SnO_2 and SnO_2 has no effect on the crystalline lattice of platinum. On

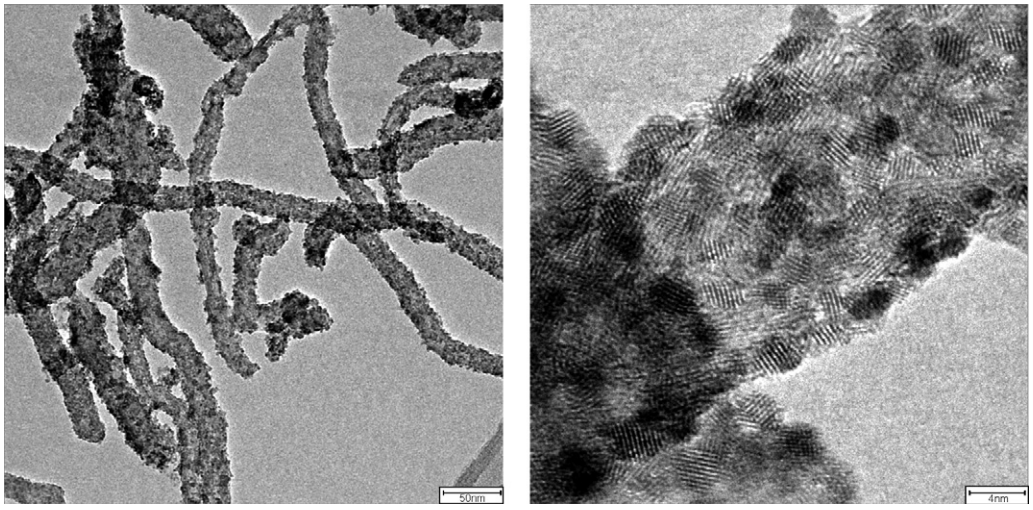

Fig. 3. TEM and HRTEM images of Pt–S-SnO_2/MWCNT composites.

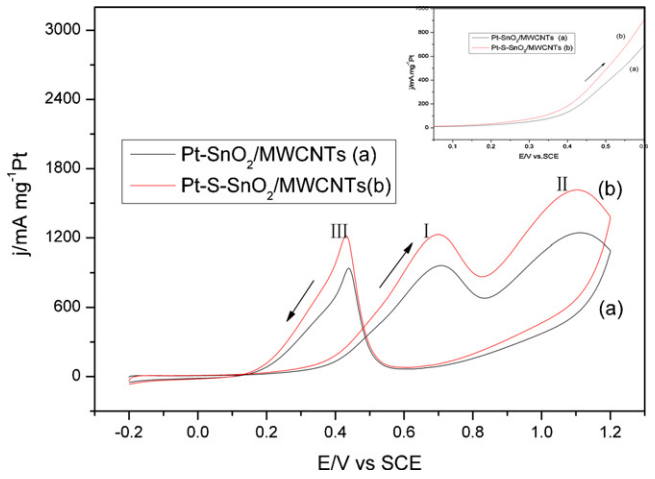

Fig. 5. Cyclic voltammograms of (a) Pt–SnO_2/MWCNTs and (b) Pt–S-SnO_2/MWCNTs electrode in 0.1 M $HClO_4$ + 0.5 M C_2H_5OH solutions at a scan rate of 50 mV s^{-1}. The insert figure shows the enlarged parts of curves (a) and (b) in the potential range 0.05–0.6 V in the positive going-scan.

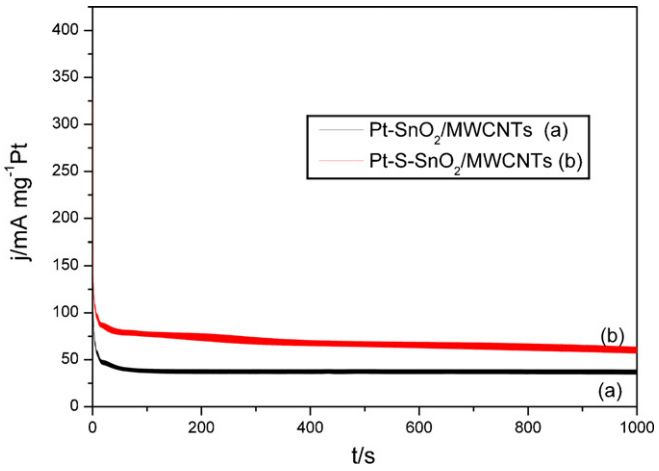

Fig. 6. Chronoamperometry curves for ethanol oxidation in 0.1 M $HClO_4$ + 0.5 M C_2H_5OH on (a) Pt–SnO_2/MWCNTs and (b) Pt–S-SnO_2/MWCNTs catalysts at 0.4 V and room temperature.

the other hand, the diffraction peaks at ca. 27°, 32°, 52°, and 66° in the XRD patterns of S-SnO_2/MWCNTs and SnO_2/MWCNTs can be attributed to the (1 1 0), (1 0 1), (2 1 1) and (3 0 1) faces of tetragonal SnO_2, respectively. The breadth of the XRD peaks also indicated that small Pt and S-SnO_2 crystallites were obtained. The average crystallite size of Pt nanoparticles calculated from the Pt (3 1 1) reflection plane by using the Debye–Scherrer equation was about 3.0 nm for Pt–S-SnO_2/MWCNTs and 3.2 nm for Pt– SnO_2/MWCNTs, in good agreement with the values obtained by HRTEM analysis. The average crystallite size of SnO_2 nanoparticles calculated from the SnO_2 (2 1 1) reflection plane by using the Debye–Scherrer equation was about 2.6 nm for S-SnO_2/MWCNTs and 3.0 nm for SnO_2/MWCNTs. The calculated values of SnO_2 crystallite size also confirmed that it is easier to form smaller nanoparticles and result in higher surface area with S-SnO_2 than with non-modified SnO_2. The same phenomenon has been reported by Matsuhashi et al. [25,26]. Matsuhashi et al. [25] speculated that acetate functions as a "place-holder" for the SO_4^{2-} groups and potentially inhibits crystallite growth.

3.4. Electrochemical properties of Pt–S-SnO_2/MWCNTs composites

The electrochemical properties of the Pt–S-SnO_2/MWCNTs catalyst for ethanol oxidation have been investigated by cyclic voltammetry (CV) in 0.1 M $HClO_4$ + 0.5 M CH_3CH_2OH aqueous solution and the corresponding results are shown in Fig. 5 (curve b). To further investigate the role played by the sulfated SnO_2 coating, we also present the cyclic voltammogram of the Pt–SnO_2/MWCNTs catalyst with the same Pt loading (curve a, Fig. 5) for comparison. The typical CVs of ethanol oxidation can be observed on both electrodes. Three oxidation peaks of ethanol oxidation are observed, the same as reported in the literature [31,32]. According to the results reported in the literature [33], ethanol oxidation mainly led to acetic acid via acetaldehyde. The exact products for these peaks are still unclear. From Fig. 5, it can clearly be seen that the current density of the Pt–S-SnO_2/MWCNTs catalyst is higher than that of the Pt–SnO_2/MWCNTs catalyst and that this difference becomes more pronounced as the potential increases. The ethanol oxidation activity could be reflected by the magnitude of the anodic peak current in the forward scan. The peak current densities (mass activities) obtained at the potential of about 0.7 V (peak I) in the forward scan for Pt–S-SnO_2/MWCNTs and Pt–SnO_2/MWCNTs catalysts are 1227.5 mA mg^{-1} Pt and 962.5 mA mg^{-1} Pt, respectively, which have been normalized to the Pt loading. The Pt–S-SnO_2/CNT catalyst displays a current density 1.28 times higher than that of the Pt–SnO_2/MWCNTs catalyst. The onset potential is shown more clearly, in the insert figure in Fig. 5. From the insert figure in Fig. 5, it can be observed that the onset potential of ethanol oxidation for the Pt–S-SnO_2/MWCNTs catalyst is about 0.16 V, which is lower than the corresponding value for the Pt–SnO_2/MWCNTs catalyst (0.2 V). The value (0.16 V) is lower than that reported by Song et al. [13] and Pang et al. [19], but higher than that reported by Lamy et al. [34,35]. Current density and onset potential of ethanol oxidation are two important parameters to evaluate the performance of electro-catalysts. The lower onset potential and higher peak current density of ethanol oxidation for the Pt–S-SnO_2/MWCNTs catalyst indicate that it is superior to the Pt–SnO_2/MWCNTs catalyst. All these phenomenon may be explained as follows: (i) sulfated SnO_2, also known as solid superacid, had a smaller particle size than non-modified SnO_2 [25,26]. So the Pt nanoparticles supported on sulfated SnO_2 have a high surface area. Besides, the Pt on sulfated SnO_2 can donate and accept protons. Therefore, the Pt utilization can be increased. (ii) SnO_2 can dissociate H_2O under lower potentials than Pt. The sulfated SnO_2 holds more water than the non-sulfated SnO_2. So sulfated SnO_2 can supply more oxygen-containing species (OHads), which can conveniently react with the CO-like species produced from ethanol oxidation to free Pt active sites. (iii) It has been reported that the catalytic activity of Pt nanoparticles deposited on tin oxides could be enhanced dramatically due to the strong chemical interaction between Pt and SnO_2 [36]. The interactions between Pt and SnO_2 can be confirmed by the XPS results that we reported before [20]. Sulfated SnO_2 is a proton conductor, and as support for a Pt catalyst may facilitate the utilization of the catalyst for ethanol oxidation.

The electrochemical stability of the Pt–SnO_2/MWCNTs and Pt–S-SnO_2/MWCNTs catalysts for ethanol oxidation was investigated by chronoamperometric experiments at room temperature. The current–time curves for the Pt–SnO_2/MWCNTs and Pt–S-SnO_2/MWCNTs catalysts in 0.1 M $HClO_4$ + 0.5 M CH_3CH_2OH aqueous solution at 0.4 V are shown in Fig. 6. The initial high current corresponds mainly to double-layer charging. The currents decay with time in a first-order exponential decay and reach an apparent steady state within 500 s. In general, ethanol was continuously oxidized on the catalyst surface when the potential was fixed at 0.4 V. Many reaction intermediates such as COads would begin to accumulate if the kinetics of their removal could not keep pace

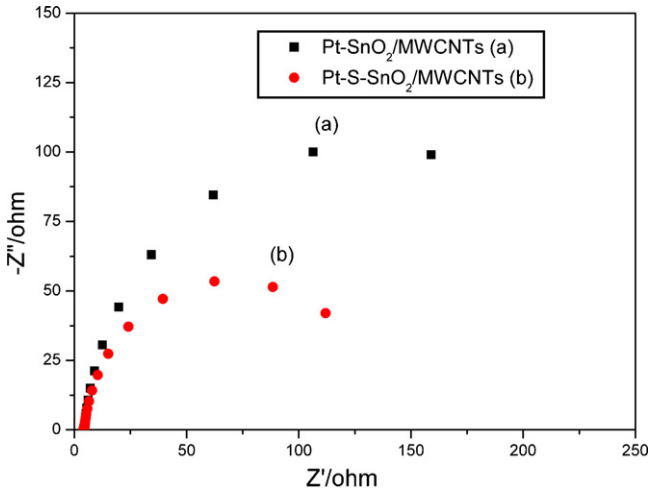

Fig. 7. Nyquist plots of impedance spectroscopy for ethanol oxidation on (a) Pt–SnO_2/MWCNTs and (b) Pt–S-SnO_2/MWCNTs electrode in 0.1 M $HClO_4$ + 0.5 M CH_3CH_2OH aqueous solution at 0.5 V.

with that of ethanol oxidation. A gradual decay of current density with time implies that the catalyst has good anti-poisoning ability. As shown in Fig. 6, the current density of ethanol oxidation on the Pt–S-SnO_2/MWCNTs electrode decreases slowly for the whole time, whereas the corresponding decay on the Pt–SnO_2/MWCNTs electrode is fast. This is an indication that the anti-poisoning ability of Pt–S-SnO_2/MWCNTs is better than that of Pt–SnO_2/MWCNTs, consistent with the result shown in Fig. 5. The steady-state current densities at the end of 1000 s for Pt–S-SnO_2/MWCNTs and Pt–SnO_2/MWCNTs are 63.7 mA mg^{-1} Pt and 34.4 mA mg^{-1} Pt, respectively. The current density for Pt–S-SnO_2/MWCNTs catalysts remains higher than that for Pt–SnO_2/MWCNTs throughout all the ranges up to 1000 s, indicating the former catalysts are more active than the latter for ethanol oxidation. The improved anti-poisoning ability and catalytic activity of Pt–S-SnO_2/MWCNTs catalyst would be due to both the strengthening of the bifunctional mechanism and the high electron and proton conductivity of the S-SnO_2/MWCNTs composites, as is consistent with the cyclic voltammetry results.

All the above CV and chronoamperometry results indicate that the Pt–S-SnO_2/MWCNTs catalyst exhibits higher catalytic activity for ethanol oxidation than the Pt–SnO_2/MWCNTs catalyst. This can be confirmed further by the results of the electrochemical impedance spectroscopy measurements that were carried out on these catalysts at a potential of 0.5 V. Electrochemical impedance spectroscopy (EIS) is a powerful diagnostic tool that can be used to investigate the intrinsic behavior of ethanol oxidation by the catalysts. Fig. 7 shows the Nyquist plots for the Pt–S-SnO_2/MWCNTs and Pt–SnO_2/MWCNTs catalysts in solutions containing 0.5 M CH_3CH_2OH and 0.1 M $HClO_4$. The Nyquist plots consist of left semicircle and right semicircle for each sample. The diameter of the right semicircle is a measure of the charge transfer resistance (Rct), which is related to the reaction kinetics of charge transfer during the ethanol oxidation process on the Pt–S-SnO_2/MWCNTs and Pt–SnO_2/MWCNTs catalysts [37,38]. A smaller diameter of semicircle means less charge transfer resistance. It can be seen that the diameter of semicircle for Pt–S-SnO_2/MWCNTs composites is smaller than that for Pt–SnO_2/MWCNTs, indicating that the ethanol oxidation occurs more easily in Pt–S-SnO_2/MWCNTs. The addition of sulfated SnO_2 to Pt/MWCNTs appears to decrease the charge transfer resistance more than the addition of non-sulfated SnO_2 does, indicating an improvement in the kinetics of ethanol oxidation using the Pt–S-SnO_2/MWCNTs catalyst instead of the Pt–SnO_2/MWCNTs catalyst. This may be ascribed to the better electron and proton conductivity of the S-SnO_2/MWCNTs support than that of the SnO_2/MWCNTs support. The decrease in the diameter of semicircle in the Nyquist plots indicates the improved catalytic activities of Pt–S-SnO_2/MWCNTs composites in agreement with the cyclic voltammetry and chronoamperometry results.

4. Conclusions

A Pt catalyst supported on sulfated SnO_2 modified MWCNTs was prepared by using the improved sol–gel and ethylene glycol reduction methods. FT-IR analysis revealed that SOx exists on the surface of the sulfated SnO_2/MWCNTs composites. HRTEM and XRD show that the Pt nanoparticles were uniformly adsorbed on the sulfated SnO_2 modified MWCNTs composites. Electrochemical studies using cyclic voltammetry, chronoamperometry and impedance spectroscopy demonstrate that Pt–S-SnO_2/MWCNTs exhibited higher catalytic activity for ethanol oxidation than Pt–SnO_2/MWCNTs did. The influence of sulfated SnO_2 on Pt activity towards ethanol oxidation may be due to the bifunctional mechanism, the synergetic interaction between Pt and S-SnO_2, and intrinsic mechanisms such as high proton and electron conductivity, which can decrease the charge transfer resistance and increase the rate and current density of ethanol oxidation. The results presented here indicate that the Pt–S-SnO_2/MWCNTs catalyst might be a promising and less expensive ethanol oxidation catalyst in direct ethanol fuel cells. Furthermore, the sulfated metal oxide is not limited to S-SnO_2, and most superacids that are stable in acidic solution can be used.

Acknowledgements

The authors gratefully acknowledge the financial support from the National Science Foundation of China (Nos. 20876013, 50674006 and Key Program No. 20636060) and International S&T Cooperation Program of China (Nos. 2009DFA63120 and 2006DFA61240).

References

[1] S.Q. Song, W.J. Zhou, Z.H. Zhou, L.H. Jiang, G.Q. Sun, Q. Xin, V. Leontidis, S. Kontou, P. Tsiakaras, Int. J. Hydrogen Energy 30 (2005) 995–1001.
[2] K. Fatih, V. Neburchilov, V. Alzate, R. Neagu, H. Wang, J. Power Sources 195 (2010) 7168–7175.
[3] E. Ribadeneira, B.A. Hoyos, J. Power Sources 180 (2010) 238–242.
[4] E. Antolini, J. Power Sources 170 (2007) 1–12.
[5] F. Vigier, C. Coutanceau, A. Perrard, E.M. Belgsir, C. Lamy, J. Appl. Electrochem. 34 (2004) 439–446.
[6] J. Riberio, D.M. dos Anjos, K.B. Kokoh, C. Coutanceau, J.M. Léger, P. Olivi, A.R. de Andrade, G. Tremiliosi-Filho, Electrochim. Acta 52 (2007) 6997–7006.
[7] R. Ianniello, V.M. Schmidt, J.L. Rodríguez, E. Pastor, J. Electroanal. Chem. 471 (1999) 167–179.
[8] M.L. Calegaro, H.B. Suffredini, S.A.S. Machado, L.A. Avaca, J. Power Sources 156 (2006) 300–305.
[9] C.W. Xu, P.K. Shen, X.H. Ji, R. Zeng, Y.L. Liu, Electrochem. Commun. 7 (2005) 1305–1308.
[10] C.W. Xu, P.K. Shen, J. Power Sources 142 (2005) 27–29.
[11] D.Y. Zhang, Z.F. Ma, G. Wang, K. Konstantinov, X. Yuan, H.K. Liu, Electrochem. Solid State Lett. 9 (2006) A423–A426.
[12] Y.X. Bai, J.J. Wu, X.P. Qiu, J.Y. Xi, J.S. Wang, J.F. Li, W.T. Zhu, L.Q. Chen, Appl. Catal. B: Environ. 73 (2007) 144–149.
[13] H.Q. Song, X.P. Qiu, F.S. Li, W.T. Zhu, L.Q. Chen, Electrochem. Commun. 9 (2007) 1416–1421.
[14] H. Song, X. Qiu, F. Li, Appl. Catal. A: Gen. 364 (2009) 1–7.
[15] L.H. Jiang, G.Q. Sun, Z.H. Zhou, S.G. Sun, Q. Wang, S.Y. Yan, H.Q. Li, J. Tian, J.S. Guo, B. Zhou, Q. Xin, J. Phys. Chem. B 109 (2005) 8774–8778.
[16] L.H. Jiang, Z.H. Zhou, W.Z. Li, W.J. Zhou, S.Q. Song, H.Q. Li, G.Q. Sun, Q. Xin, Energy Fuels 18 (2004) 866–871.
[17] A. Kowal, M. Li, M. Shao, K. Sasaki, M. Vukmirovic, J. Zhang, N. Marinkovic, P. Liu, A. Frenkel, R. Adzic, Nat. Mater. 8 (2009) 325–330.
[18] A. Kowal, S. Gojkovičí, K.S. Lee, P. Olszewski, Y.E. Sung, Electrochem. Commun. 11 (2009) 724–727.
[19] H.L. Pang, J.P. Lu, J.H. Chen, C.T. Huang, B. Liu, X.H. Zhang, Electrochim. Acta 54 (2009) 2610–2615.
[20] X.W. Zhang, H. Zhu, Z.J. Guo, Y.S. Wei, F.H. Wang, Int. J. Hydrogen Energy 35 (2010) 8841–8847.
[21] M.A. Navarra, F. Croce, B. Scrosati, J. Mater. Chem. 17 (2007) 3210–3215.

[22] M.A. Navarra, C. Abbati, B. Scrosati, J. Power Sources 183 (2008) 109–113.
[23] Z.M. Wu, G.Q. Sun, W. Jin, H.Y. Hou, S.L. Wang, Q. Xin, J. Membr. Sci. 313 (2008) 336–343.
[24] Z.M. Wu, G.Q. Sun, W. Jin, H.Y. Hou, S.L. Wang, Q. Xin, Int. J. Hydrogen Energy 35 (2010) 12461–12468.
[25] H. Matsuhashi, H. Miyazaki, Y. Kawamura, H. Nakamura, K. Arata, Chem. Mater. 13 (2001) 3038–3042.
[26] H. Matsuhashi, H. Miyazaki, K. Arata, Chem. Lett. 30 (2001) 452–453.
[27] S.Q. Song, Y. Wang, P.K. Shen, J. Power Sources 170 (2007) 46–49.
[28] H.F. Guo, P. Yan, X.Y. Hao, Z.Z. Wang, Mater. Chem. Phys. 112 (2008) 1065–1068.
[29] M.K. Lam, K.T. Lee, A.R. Mohamed, Appl. Catal. B: Environ. 93 (2009) 134–139.
[30] L.K. Noda, R.M. de Almeida, L.F.D. Probst, N.S. Goncalves, J. Mol. Catal. A: Chem. 225 (2005) 39–46.
[31] N. Fujiwara, K.A. Friedrich, U. Stimming, J. Electroanal. Chem. 472 (1999) 120–125.
[32] H. Hitmi, E.M. Belgsir, J.M. Léger, C. Lamy, R.O. Lezna, Electrochim. Acta 39 (1994) 407–415.
[33] H.Q. Li, G.Q. Sun, L. Cao, L.H. Jiang, Q. Xin, Electrochim. Acta 52 (2007) 6622–6629.
[34] C. Lamy, S. Rousseau, E.M. Belgsir, C. Coutanceau, J.M. Léger, Electrochim. Acta 49 (2004) 3901–3908.
[35] S. Rousseau, C. Coutanceau, C. Lamy, J.M. Léger, J. Power Sources 158 (2006) 18–24.
[36] N. Kamiuchi, T. Matsui, R. Kikuchi, K. Eguchi, J. Phys. Chem. C 111 (2007) 16470–16476.
[37] J.H. Kim, H.Y. Ha, I.H. Oh, S.A. Hong, H.N. Kim, H.I. Lee, Electrochim. Acta 50 (2004) 801–806.
[38] J. Otomo, X. Li, T. Kobayashi, C.J. Wen, H. Nagamoto, H. Takahashi, J. Electroanal. Chem. 573 (2004) 99–109.